energies

MDPI

Article

Experimental Data-Driven Parameter Identification and State of Charge Estimation for a Li-Ion Battery Equivalent Circuit Model

Hui Pang * and Fengqi Zhang

School of Mechanical and Precision Instrument Engineering, Xi'an University of Technology, Xi'an 710048, China; zfqdy@126.com

* Correspondence: huipang@163.com; Tel.: +86-29-8231-2599

Received: 9 March 2018; Accepted: 17 April 2018; Published: 24 April 2018

Abstract: It is well known that accurate identification of the key state parameters and State of Charge (SOC) estimation method for a Li-ion battery cell is of great significance for advanced battery management system (BMS) of electric vehicles (EVs), which further facilitates the commercialization of EVs. This study proposed a systematic experimental data-driven parameter identification scheme and an adaptive extended Kalman Filter (AEKF)-based SOC estimation algorithm for a Li-Ion battery equivalent circuit model in EV applications. The key state parameters of Li-ion battery cell were identified based on the second-order resistor capacitor (RC) equivalent circuit model and the experimental battery test data using genetic algorithm (GA). Meanwhile, the proposed parameter identification procedure was validated by carrying out a comparative study of the simulated and experimental output voltage under the same input current profile. Then, SOC estimation was performed based on the AEKF algorithm. Finally, the effectiveness and feasibility of the proposed SOC estimator was verified by loading different operating profiles.

Keywords: electric vehicles; Li-ion battery cell; parameter identification; sate of charge; extended Kalman filter

1. Introduction

In recent years, Li-Ion battery (LIB) has been widely used in electric vehicles (EVs) and hybrid electric vehicles (HEVs) due to their high energy density, long cycle-life, low self-discharge and high specific power [1,2]. For EVs and HEVs, the accurate state parameters and state-of-charge (SOC) of the LIB is of great significance in real-time control and high-performance operation for advanced battery management system (BMS) of EVs because these parameters are often used to implement the optimum control of charging and discharging process, which is not only beneficial for efficient vehicular BMS, but also for the diagnosis and prognosis of the LIB behavior. Therefore, to manage the LIB more efficiently and improve the battery performance, it is necessary to obtain the inner state parameters and to make an accurate SOC estimation for the battery accurately.

A large quantity of battery SOC estimation methods based on Li-Ion battery equivalent circuit mode (ECM) have been reported in the literature [3–12], which can be classified as coulomb counting [3–5], open circuit voltage (OCV)-based method [6,7], and model-based method [8–12]. Among these studies, the model-based filtering estimation methods such as the Kalman filter (KF) and the related extended Kalman filter (EKF) have been extensively applied due to their closed-loop nature and concerning various uncertainties. For instances, Plett et al. [13–15] firstly adopted EKF to estimate SOC using different battery models. However, the Kalman filter-based algorithm strongly depends on the precision of the battery model and the predetermined variables of the system noise such as

mean value, relevance and covariance. In addition, Feng and Verbrugge et al. in [7,16] integrated EKF algorithm with recursive least squares to identify the related parameters online. Nevertheless, the battery states information with a constant input current may not be completely observable and even an inappropriate information matrix of the system noise will lead to some remarkable errors and divergence [17]. More specifically, the current EKF-based SOC estimation approaches result in a rather moderate improvement as compared to the commonly-used KF, while the estimation errors caused by the local linearization increase greatly when the battery model has significant nonlinearity. Moreover, the EKF method requires calculation of the Jacobian matrix, which may result in instability of the filter for a strongly nonlinear LIB system.

To overcome the drawbacks in using the EKF-based SOC estimation approaches, an adaptive extended Kalman filter (AEKF)-based method has been developed to deal with the problem of choosing the covariance to improve the estimation performance. An online parameter identification method was used in [18] to estimate the OCV. He et al. in [19] conducted a comparison of the SOC estimation between the AEKF-based OCV estimator and AEKF-based SOC estimator. The results showed that this method had desirable performance with an acceptable accuracy. Additionally, the AEKF algorithm has been employed for the parameters identification and SOC estimation of Li-Ion battery in [11,20–22], wherein the process covariance matrix is adaptively updated online with a dedicated estimator. However, the battery parameters may vary with the different operation conditions, which are always ignored in the previous study. The robustness of these SOC estimation methods were not sufficiently discussed under different aging levels and input current profiles. To this end, a data-driven parameter identification method [23,24] was proposed to update the model parameters in real-time, and the adaptive SOC estimator was established with an adaptive extended Kalman filter, which provided significant inspirations for the follow-up study on parameter identification and SOC estimation for a Li-Ion Battery based on first-order and/or second-order ECM.

Based on the above discussions, this paper proposes an experimental data-driven parameter identification and SOC estimation for a second-order RC equivalent circuit model of Li-Ion battery. The key contribution of this work is that a test data-driven parameter identification procedure was presented using genetic algorithm, which only yields higher computation efficiency and reached a fast convergence during the optimized process. Moreover, an AEKF-based SOC estimator was developed using the two typical driving cycles with different battery aging levels. The results showed that this SOC estimator can achieve good performance in terms of estimation accuracy and robustness with respect to EKF.

The remainder of this paper is organized as follows: Section 2 presents the second-order RC equivalent circuit model of Li-Ion battery. Section 3 addresses the experimental data-driven parameter identification and validation results. The AEKF-based SOC estimation method is introduced in Section 4. The conclusions of this study are made in Section 5.

2. An Equivalent Circuit Model of Li-Ion Battery

Due to advantages such as well-describing the cell dynamic behaviors of Li-ion battery and less computational resource requirements, the second-order ECM is selected to model a Li-ion battery, which has been extensively employed in the literature [25–28]. As shown in Figure 1, the second-order RC battery model is composed of an open-circuit voltage (OCV) denoted by $U_{oc}(SOC)$, a resistance R_0, and two parallel RC networks connected in series (i.e., R_1-C_1 and R_2-C_2). The resistance R_0 is the Ohmic resistances caused by the accumulation and dissipation of charge in the electrical double-layer; R_1 and C_1 are the electrochemical polarization resistance and capacitance, respectively; R_2 and C_2 are the concentration polarization resistance and capacitance, respectively; U_1 and U_2 are the polarization voltage across C_1 and C_2, respectively; $I(t)$ is the load current (supposed positive for discharge and negative for charge); and U_t is the terminal voltage.

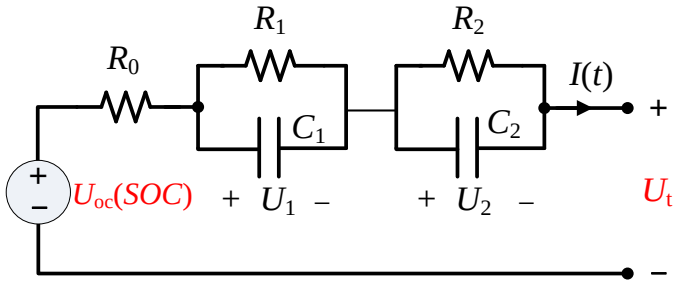

Figure 1. Schematic diagram of the second-order RC model.

According to the literature [28], the electrical behavior of the second-order RC battery model can be governed by Equation (3) as follows:

$$\begin{cases} \dot{U}_1 = -\frac{U_1}{R_1C_1} + \frac{1}{C_1}I(t) \\ \dot{U}_2 = -\frac{U_2}{R_2C_2} + \frac{1}{C_2}I(t) \\ U_t = U_{oc}(SOC) - U_1 - U_2 - I(t)R_0 \end{cases} \tag{1}$$

Generally, the battery SOC is defined as a ratio of the remaining capacity over the nominal available capacity, and the SOC calculated by Coulomb Counting can be expressed in the discrete form as [29]:

$$SOC(k+1) = SOC(k) - \frac{\eta \Delta t I(k)}{Q_N} \tag{2}$$

where $SOC(k+1)$ and $SOC(k)$ are the SOC at (k + 1)th and kth sampling time, respectively; η is the Coulomb efficiency that is assumed to be 1 at charging and 0.98 at discharging as the battery works in a limited current range; Q_N is the nominal capacity; and Δt represents the sampling interval.

It should be noted that $U_{oc}(SOC)$ is usually a nonlinear function of SOC at the same temperature, which will be demonstrated in Section 3.1. Define the state vector of Equation (1) as $x = \begin{bmatrix} SOC & U_1 & U_2 \end{bmatrix}^T$, and the current $I(t)$ and terminal voltage U_t as the input and output variables, respectively, then, using the zero-order hold discretization method in [30], the discrete-time state equations of the second-order RC battery model can be written as:

$$\begin{cases} x_{k+1} = f(x_k, u_k) + \omega_k \\ y_k = h(x_k, u_k) + v_k \end{cases} \tag{3}$$

where x_k denotes the immeasurable state vector at time step k, u_k(=$I(k)$) denotes the input vector, y_k(=$U_t(k)$) is the observed output voltage, and ω_k and v_k are an independent and zero mean Gaussian white noise signals, respectively. $f(x_k, u_k)$ is the nonlinear system process function, and $h(x_k, u_k)$ is the nonlinear measurement function, which can be expressed as:

$$f(x_k, u_k) = \begin{bmatrix} U_1(k)\exp\left(-\frac{\Delta t}{R_1C_1}\right) + I(k)R_1\left(1 - \exp(-\frac{\Delta t}{R_1C_1})\right) \\ U_2(k)\exp\left(-\frac{\Delta t}{R_2C_2}\right) + I(k)R_2\left(1 - \exp(-\frac{\Delta t}{R_2C_2})\right) \\ SOC(k) - \frac{\eta \Delta t I(k)}{Q_n} \end{bmatrix} \tag{4}$$

$$h(x_k, u_k) = U_{oc}(SOC(k)) - U_1(k) - U_2(k) - I(k)R_0 \tag{5}$$

3. Experimental Data-Driven Parameter Identification

The experimental data-driven parameter identification in this section starts with the battery experimental investigation, which is utilized to test the characteristics of the battery, identify the Li-ion battery parameters and verify the effectiveness of the proposed SOC estimation method. It is noted

that the identified parameters include R_0, R_1, C_1, R_2, C_2 and the nonlinear function $U_{oc}(SOC)$ for the second-order RC equivalent circuit model shown in Figure 1.

3.1. Battery Experimental Setup

The experiment data of Li-ion battery used for this study were acquired through the test bench shown in Figure 2, which is composed of an Arbin BT2000 Cycler with MITS Pro soft (ARBIN INSTRUMENS, College Station, TX, USA), a well-controlled temperature chamber for environment control and a host computer for the human–machine interface and test data storage, as well as the Li-ion battery cells. It is noted that the test cells are SONY lithium nickel-manganese-cobalt oxide (NMC) battery (SONY Inc, Tokyo, Japan) with graphite anode. According to the producer's specification, the battery nominal capacity is 2 Ah, and the nominal voltage is 3.7 V. Lower and upper cut-off voltage is 2.5 V and 4.2 V, respectively. The temperature is controlled by a constant temperature battery experimental chamber. At different given temperatures (5 °C, 25 °C, 30 °C, and 40 °C), the battery cells are relatedly cycled. The measured signals including input current, output voltage, the battery's input current and terminal voltage, the battery's OCV, and SOC corresponded to OCV are recorded by Arbin BT2000 (ARBIN INSTRUMENS, College Station, TX, USA) under different aging states (in the order of hybrid pulse power characterization (HPPC), standard US06 driving cycle (US06) and 1C-rate discharge operating condition), and then exported to store in mat files for Matlab software (Matlab 2016b, MathWorks Inc, Natick, MA, USA) processing.

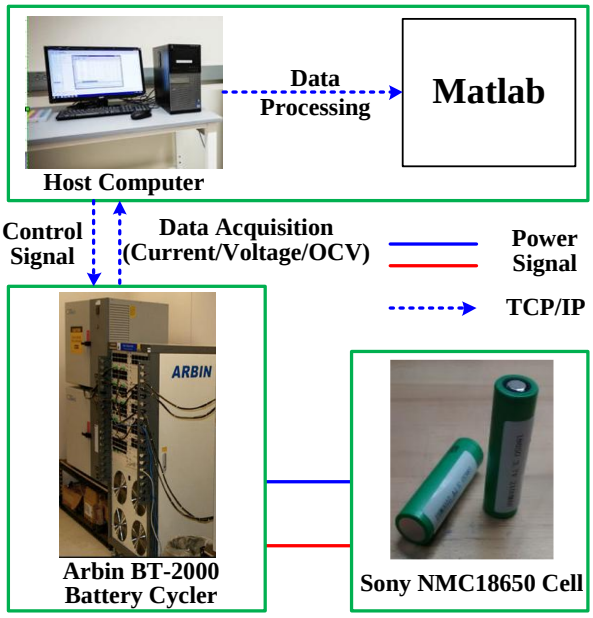

Figure 2. Test configuration of Li-ion battery test bench.

With the complete battery OCV–SOC test data at different temperatures (5 °C, 25 °C, 30 °C, and 40 °C), we can obtain the plots shown in Figure 3. It is seen in Figure 3 that the temperature variation leads to very small changes in the OCV, thus the effect of temperature on the cell OCV during discharge progress was neglected in this work for simplification. In other words, the temperature has little effect on the variation of OCV–SOC curves. As a result, for this study, the test data for 30 °C were used as the reference to perform the parameters identification, and the other datasets were utilized in the model validation and SOC estimation. From [15,28], the collected test data at 30 °C were used to build the OCV–SOC function using the simplified electrochemical function (Equation (6)).

After some calculations, the corresponding model-fitting coefficients are $K_0 = 3.3984$, $K_1 = 0.4549$, $K_2 = 0.0078$, $K_3 = 0.0142$, and $K_4 = 0.0857$. Moreover, the comparisons of the experimental and fitted

OCV–SOC curves, as well as the corresponding OCV test data at 30 °C for NMC battery are presented in Figure 4. It is obvious that the fitted nonlinear function can well simulate the OCV–SOC relationship.

$$U_{oc}(SOC) = K_0 + K_1 \cdot SOC + \frac{K_2}{SOC} + K_3 \cdot \ln SOC + K_4 \cdot \ln(1 - SOC) \quad (6)$$

where K_i (i = 0, 1, 2, 3, 4) are the coefficients to be determined that could make $U_{oc}(SOC)$ fit the SOC-OCV test data well.

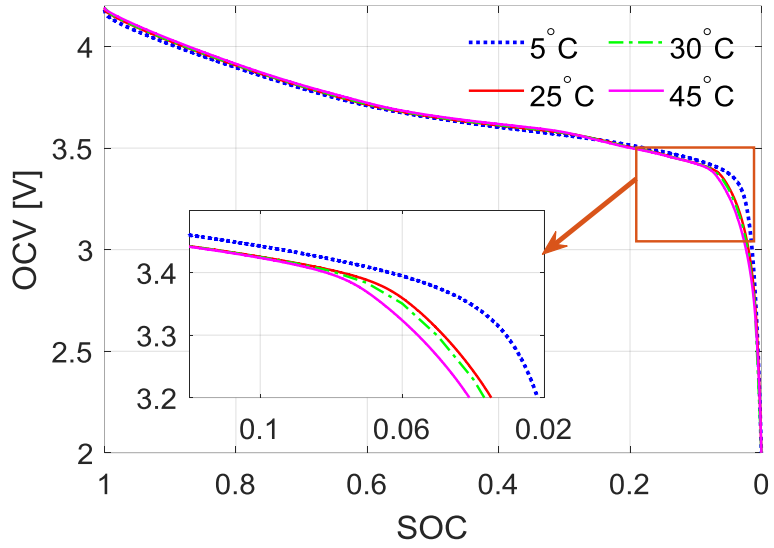

Figure 3. The experimental OCV–SOC curves for NMC battery at different temperatures.

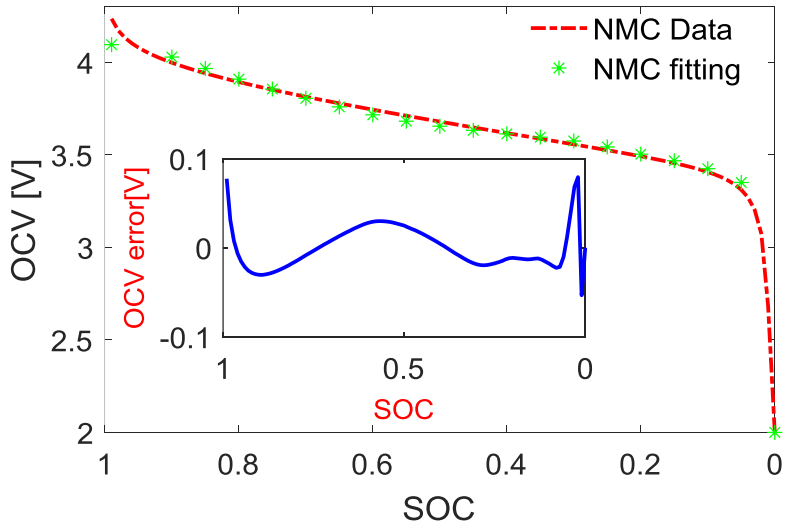

Figure 4. The experimental and fitted OCV–SOC curves and the variation of OCV error at 30 °C.

3.2. Parameter Identification Procedure

To identify the parameters of Li-ion battery model as R_0, R_1, C_1, R_2, and C_2, the sum of squares errors of the measured data denoted as U_{exp} and the simulated data denoted as U_{sim} for the terminal voltage at each sampling point of input current is chosen as the objective function, which is represented by L^2 as follows:

$$L^2 : \min_{\theta} \sum_{i=1}^{N} \left[U_{exp}(t_i) - U_{sim}(\theta, t_i) \right]^2 \quad (7)$$

where N is the number of samples in the input current and θ is the identified parameter vector shown in Table 1.

Table 1. The identified parameters for second-order RC ECM of LIB.

Symbol	Unit	Search Ranges	Identified Values
R_0	Ω	[0.050, 0.150]	0.0904
R_1	Ω	[0.005, 0.015]	0.0097
R_2	Ω	[0.005, 0.015]	0.0097
C_1	F	[500, 1000]	657.42
C_2	F	[3500, 8000]	6574.23

Figure 5 shows the flowchart of the battery parameters identification based on the genetic algorithm. The optimized flowchart starts with initializing a randomized population and each individual represents a parameter to be identified. The output voltage of second-order RC ECM is computed for individuals and their corresponding L^2 fitness is evaluated by a comparison of the experimental voltage versus the simulated voltage data. The fittest individuals in population are chosen by a fitness-weighted roulette game, and each individual's genome is recombined and randomly mutated to form a new generation population. Afterwards, the second-order RC equivalent circuit model is utilized to compute the fitness values in the new population, and the optimization process runs until either the fitness function reaches the optimal value or the iteration number exceeds a maximum number of generations.

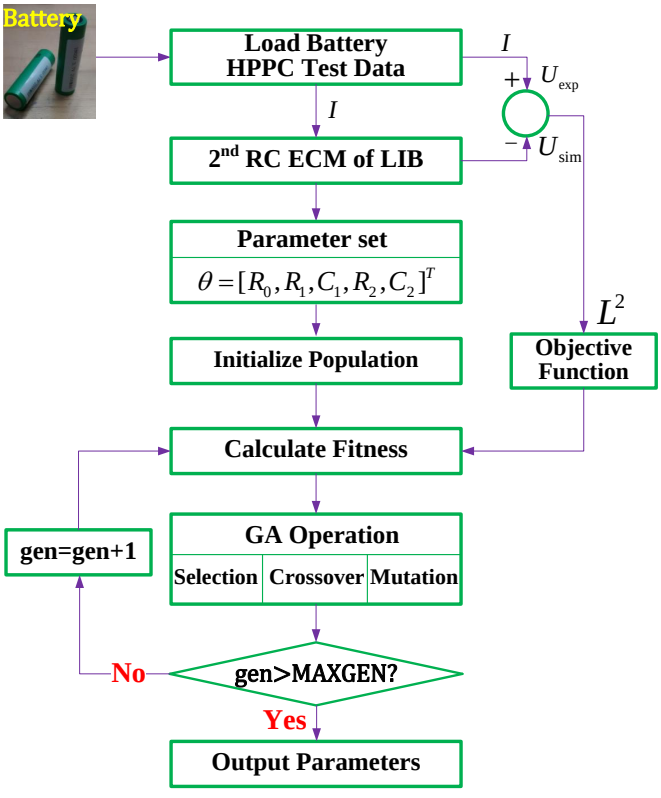

Figure 5. The flowchart of Li-ion battery parameters identification using GA.

To identify the model parameters, the hybrid pulse power characterization (HPPC) experiment is usually carried out to provide the extreme characterization of Li-Ion battery. The test current profile and terminal voltage of HPPC condition (30 °C) is presented in Figure 6 and the parameter identification is implemented by the above-mentioned GA-based flowchart. The final identified results

for the second-order RC model of Li-Ion battery are listed in Table 1. In addition, the comparisons of battery voltage between the test data and the simulated voltage with the identified parameters are shown in Figure 7.

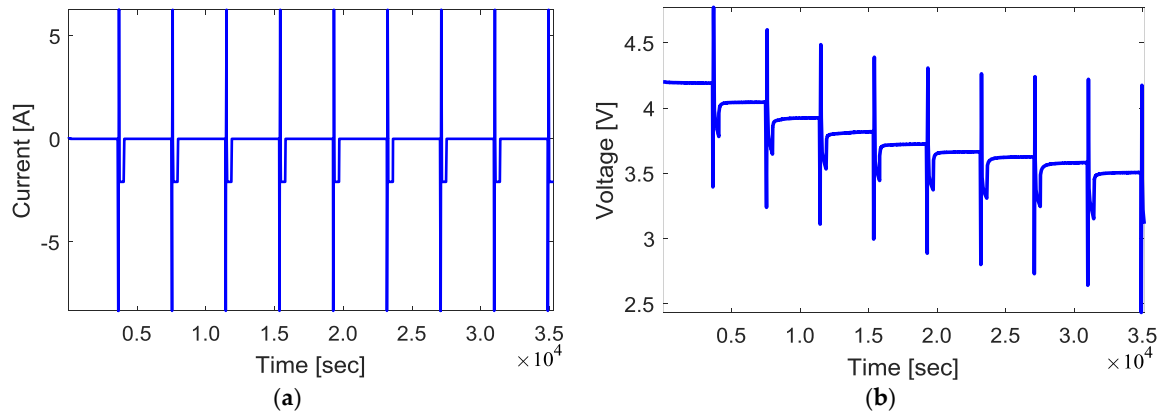

Figure 6. (**a**) Current profile; and (**b**) terminal voltage of HPPC test for the parameter identification.

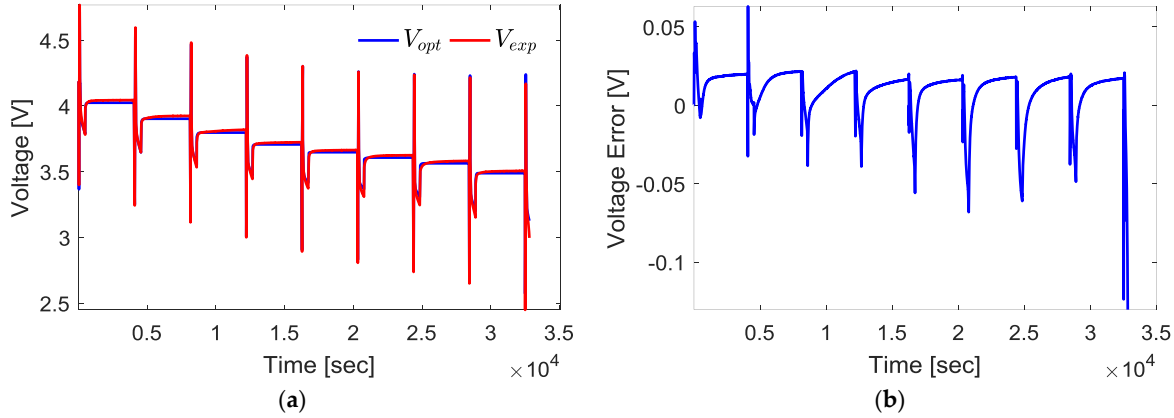

Figure 7. The identification results under HPPC condition at 30 °C: (**a**) terminal voltage of the optimal and the experimental model; and (**b**) voltage error.

3.3. Model Validation and Discussion

To assess the accuracy of the identified parameters, the experimental and simulated Li-Ion battery terminal voltages under US06 condition at 30 °C are compared and presented in Figure 8.x

In Figure 8a, the input current profiles are from the current sensor, and the comparative profiles between the estimated voltage with the identified parameters and the experimental voltage, and the normalized voltage estimation error is shown in Figure 8b,c. The maximum and mean relative errors are about 1.918% and 0.206%, respectively, which illustrates that the simulated voltage with the parameters identified by the proposed approach shows good agreement with the experimental curves at the ambient temperature of 23 °C. Therefore, the battery model can well simulate the dynamic voltage behaviors of Li-Ion battery.

To further validate the battery electrochemical behavior with the identified parameters, the comparison of the experimental voltage and the simulated voltage, as well as the voltage error under one C-rate profile at 23 °C are exhibited in Figure 9. It can be found that the simulated voltage with the parameters identified by the proposed approach show good agreement with the experimental voltage curve at the same ambient temperature, and the maximum and mean relative errors are about 2.12% and 0.244%. Moreover, the mean absolute error (MAE) and root mean squares error (RMSE) of the aforementioned test conditions during validation process are listed as in Table 2.

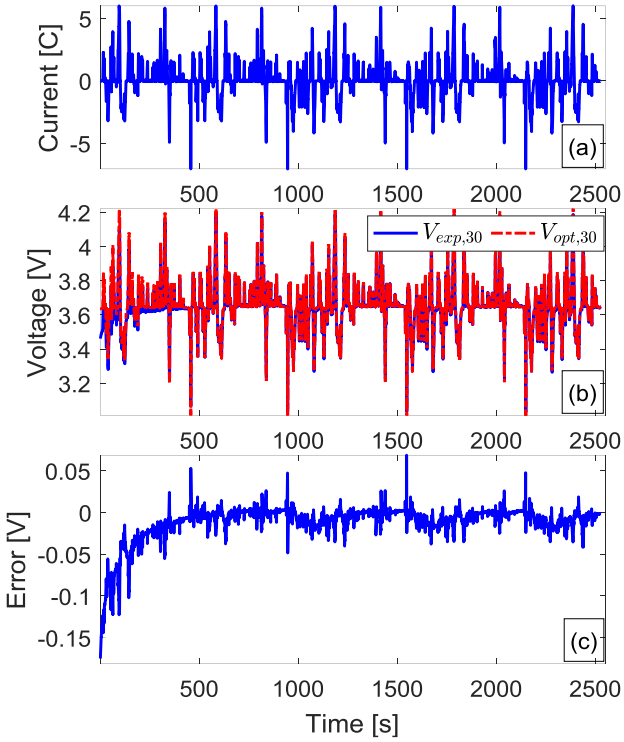

Figure 8. Validation results under US06 condition at 30 °C: (**a**) input current profile; (**b**) voltage; and (**c**) voltage error.

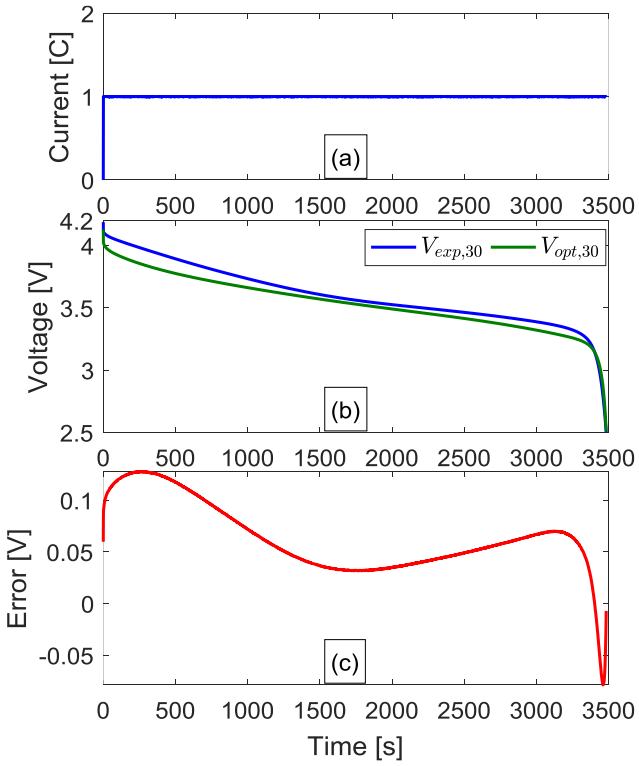

Figure 9. Validation results under 1C-rate discharge condition at 23 °C: (**a**) input current profile; (**b**) voltage; and (**c**) voltage error.

Table 2. MAE and RMSE of the simulated and measured voltage errors.

	HPPC	US06	1C
	30 °C	30 °C	30 °C
MAE [V]	0.0152	0.0131	0.0724
RMSE [V]	0.0176	0.0249	0.0655

4. SOC Estimation Method Based on the Adaptive EKF

Overall, the SOC estimation logic in this study is shown in Figure 10, where the parameter set $\theta = [R_0, R_1, C_1, R_2, C_2]^T$ and the OCV–SOC model is obtained from the discussions in Section 3. Actually, the adaptive extended Kalman filter is used to make the SOC estimation because the covariance parameters in AEKF approach are not taken as constant, but adaptively updated online with a dedicated SOC estimator [11,22,31,32], which can enhance the estimation performance with respect to the EKF. The control input of the SOC estimator is the current (HPPC and/or US06) profiles representing the behavior of Li-Ion battery during discharge or charge process, the output the SOC estimator is the SOC value estimated by the AEKF algorithm.

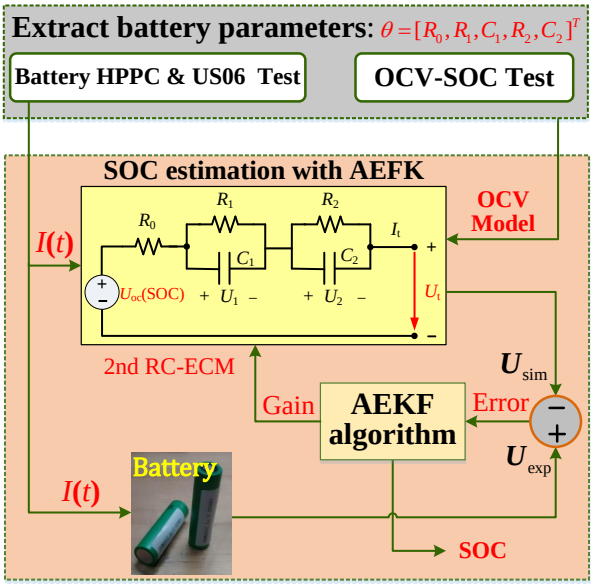

Figure 10. Flowchart of the SOC estimation logic.

4.1. AEKF Algorithm

Although Kalman filter and extended Kalman filter have been extensively introduced and employed to estimate battery SOC in recent years (e.g., [15,20,21,33,34]), its performance is strongly dependent on the accuracy of the predetermined noise matrix. Thus, it is necessary for the AEKF algorithm to adopt this problem in battery applications. To apply the AEKF for the SOC estimation, it is necessary to reform a state-space form as shown in Equation (3). The AEKF algorithm is given in Table 3.

It should be pointed out that $\hat{x}_k^-$ and $\hat{x}_k^+$ are both estimations of the same vector x_k. However, $\hat{x}_k^-$ is the estimate of x_k before the measurement y_k is considered, which is called the a priori estimate, and $\hat{x}_k^+$ is the estimate of x_k after the measurement y_k is taken into account, which is called the a posteriori estimate.

Table 3. Summary of the AEKF algorithm.

State-Space Equation of Li-ion Battery

$\begin{cases} x_{k+1} = f(x_k, u_k) + \omega_k \\ y_k = h(x_k, u_k) + v_k \end{cases}$

Step 1: Initialization

$\hat{x}_0^+ = E[x_0]$, $P_0^+ = E[(x_0 - E[\hat{x}_0^+])(x_0 - E[\hat{x}_0^+])^T]$

Step 2: Calculation

For k =1 to N perform

(1) State estimate propagation: $\hat{x}_k^- = f(\hat{x}_{k-1}^+, u_k)$

(2) Error innovation: $e_k = y_k - g(\hat{x}_k^-, u_k)$

(3) Adaptive law: $H_k = \frac{1}{M} \sum_{i=k-M+1}^{k} e_k e_k^{\mathrm{T}}$, $R_k = H_k - C_k P_k^- C_k^T$

(4) State estimation covariance: $P_k^- = A_k P_{k-1} A_k^T + Q_k$

(5) Kalman gain matrix: $K_k = P_k^- C_k^T (C_k P_k^- C_k^T + R_k)^{-1}$

(6) State estimate measurement update: $\hat{x}_k^+ = \hat{x}_k^- + K_k e_k$

(7) State covariance measurement update: $Q_k = K_k H_k K_k^T$, $P_k^+ = (I - K_k C_k) P_k^-$

Note: $A_k = \left.\frac{\partial f(x_k, u_k)}{\partial x}\right|_{x=\hat{x}_k^-}$, $C_k = \left.\frac{\partial h(x_k, u_k)}{\partial x}\right|_{x=\hat{x}_k^-}$.

end

4.2. SOC Estimation with AEKF

To employ the AEKF to estimate the SOC, we need to establish an estimator based on Equations (3)–(5) using the AEKF algorithm shown in Table 3. The state vector is $x = \begin{bmatrix} SOC & U_1 & U_2 \end{bmatrix}^T$, in which SOC is what we want to obtain. Herein, the time-varying matrices $\mathbf{A}_k$ and $\mathbf{C}_k$ can be derived from Equations (4) and (5) as follows:

$$\mathbf{A}_k = \begin{pmatrix} 0 & \exp\left(-\frac{\Delta t}{R_1 C_1}\right) & 0 \\ 0 & 0 & \exp\left(-\frac{\Delta t}{R_2 C_2}\right) \\ 1 & 0 & 0 \end{pmatrix} \tag{8}$$

$$\mathbf{C}_k = \left.\frac{\partial h}{\partial x}\right|_{\mathbf{x}=\hat{\mathbf{x}}_k} = \begin{bmatrix} -1 & -1 & \frac{dU_{\mathrm{OC}}(SOC)}{dSOC} \end{bmatrix} \tag{9}$$

where $dU_{\mathrm{OC}}(SOC)/dSOC = 0.4549 - 0.0078/SOC^2 + 0.0142/SOC - 0.0857/(1 - SOC)$ is derived from Equation (6).

With these above-mentioned matrices and functions, as well as AEKF-based SOC estimation logic shown in Figure 10, the experimental data-driven SOC estimation can be achieved. The HPPC and US06 current and voltage profiles of discharge are loaded into SONY NMC 18,650 cells and its corresponding second-order RC ECM simultaneously. Afterwards, the voltage error e_k is computed and the adaptive law H_k is employed to update $\hat{x}_k$, P_k, Q_k and K_k. Then, the updated gain is used to compensate for the state estimation error. The SOC estimation is fed back to update the parameters of the battery model for the SOC estimation at the next sampling time.

4.3. Experimental Verification Results of SOC Estimation

In this section, both of HPPC and US06 test current profiles are adopted to verify the AEKF-based SOC estimation for Li-Ion battery model in Equations (1) and (2) with the identified parameters. Firstly, with the input current of US06 condition, the battery SOC estimation values and their errors are plotted in Figure 11. It is observed in Figure 11 that the estimated SOC with EKF and AEKF can track the experimental SOC profiles well, while the maximum value of SOC error is, respectively, 3.4% and 2.6%, which illustrates that the AEKF-based algorithm has higher accuracy in estimating battery SOC.

The reason is that the AEKF-based algorithm can adjust the Kalman gain quickly according to the SOC error between the measured and estimated values.

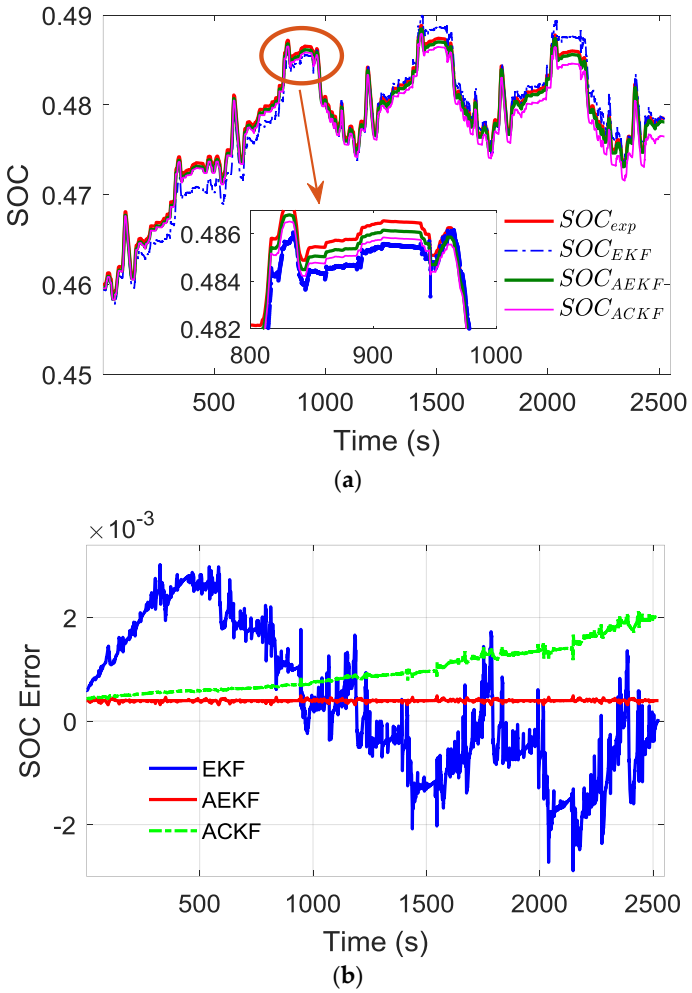

Figure 11. Validation results for SOC estimation under US06 condition at 30 °C: (**a**) SOC estimation profiles with different methods; and (**b**) SOC errors.

Secondly, the battery is operated in HPPC discharging process at 30 °C where the measured SOC is recorded and used to evaluate the accuracy of AEKF-based SOC estimation for Li-Ion battery second-order RC equivalent circuit model. Figure 12 shows the comparison of the battery SOC estimation values and their errors with EKF and AEKF algorithm, as compared with the corresponding SOC test data. It can be found that the error of SOC estimation with both EKF and AEKF algorithms under the same HPPC discharging profile are from −6.3% to +1.8%, and from −6.3% to +1.2%, respectively. It is noted that the AEKF-based SOC error yields comparatively minor fluctuations. Moreover, the root-mean-square (RMS) error of SOC estimation for EKF and AEKF algorithm is 1.02% and 0.97%, respectively. This further demonstrates that the AEKF-based SOC estimation algorithm can estimate the battery SOC with higher accuracy.

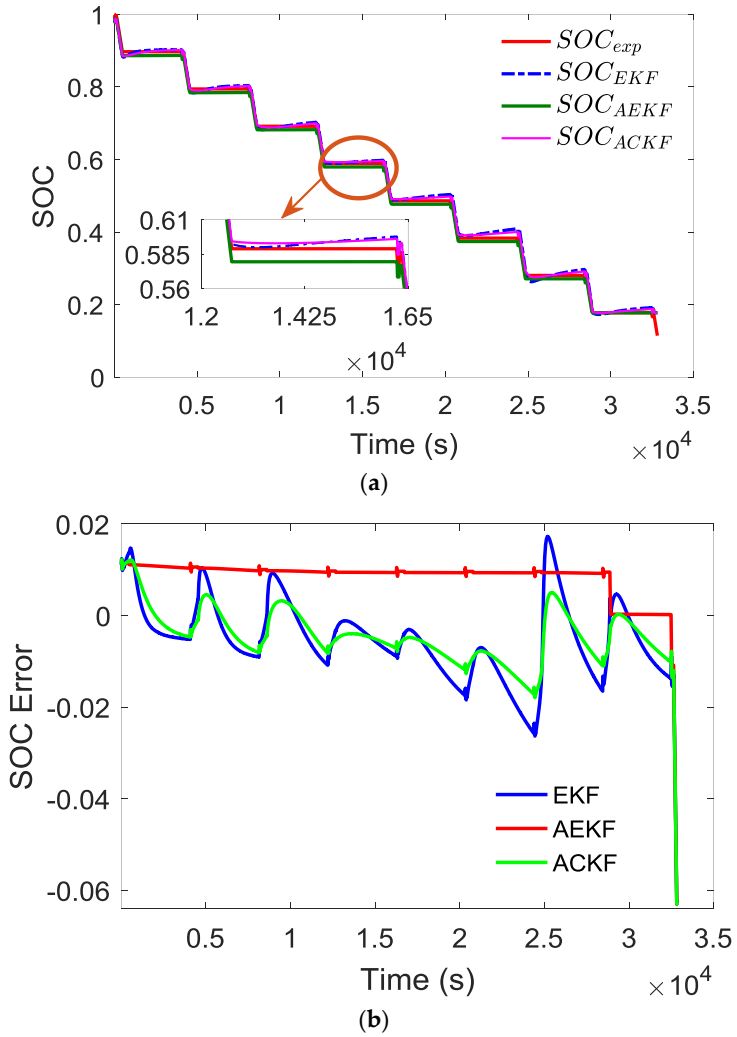

Figure 12. Validation results for SOC estimation under HPPC condition at 30 °C: (**a**) SOC estimation profiles with different methods; and (**b**) SOC errors.

5. Conclusions

In this paper, a comprehensive experimental data-driven parameter identification scheme using GA algorithm is developed and the AEKF-based SOC estimator with the identified parameters is described for the Li-ion batteries in the applications of EVs. First, the second-order RC ECM is used to simulate the nonlinear behaviors of Li-Ion battery and make SOC estimation, wherein the electrochemical model is used to build the nonlinear OCV–SOC relationship based on the experimental data of battery characterization. Second, the key state parameters of Li-ion battery are identified and validated by conducting the comparative study of the simulated and experimental output voltage under HPPC and US06 current profiles. Furthermore, the AEKF-based battery SOC estimation method is introduced to reduce the effect of the non-Gaussian system and measurements noises. The HPPC and US06 experimental data are employed to verify and evaluate the accuracy of the proposed AEKF-based SOC estimation method by comparing with the general EKF-based SOC algorithm. The comparison results confirm that the proposed SOC estimation yields good performance in terms of the SOC estimation accuracy. In future work, we will focus on the joint estimation approach considering the current dependent parameters and the aging mechanism of Li-Ion battery.

Acknowledgments: This research work was supported by the Natural Science Foundation of China under Grant 51675423.

Author Contributions: Hui Pang proposed the main idea and designed the AEKF-based SOC algorithm under literature review. Hui Pang developed the Matlab Simulink model and plots code of this study. Fengqi Zhang helped to polish the English writing of the whole manuscript.

Conflicts of Interest: The authors declared no conflict of interest.

References

1. Lu, L.G.; Han, X.B.; Li, J.Q.; Hua, J.F.; Ouyang, M.G. A review on the key issues for lithium-ion battery management in electric vehicles. *J. Power Sources* **2013**, *226*, 272–288. [CrossRef]
2. Lim, K.; Bastawrous, H.A.; Duong, V.-H.; See, K.W.; Zhang, P.; Dou, S.X. Fading Kalman filter-based real-time state of charge estimation in LiFePO4 battery-powered electric vehicles. *Appl. Energy* **2016**, *169*, 40–48. [CrossRef]
3. Ng, K.; Moo, C.S.; Chen, Y.P.; Hsieh, Y.C. Enhanced coulomb counting method for estimating state-of-charge and state-of-health of lithium-ion batteries. *Appl. Energy* **2009**, *86*, 1506–1511. [CrossRef]
4. Jeong, Y.M.; Cho, Y.K.; Ahn, J.H.; Ryu, S.H.; Lee, B.K. Enhanced Coulomb counting method with adaptive SOC reset time for estimating OCV. In Proceedings of the 2014 IEEE Energy Conversion Congress and Exposition (ECCE), Pittsburgh, PA, USA, 14–18 September 2014; pp. 1313–1318.
5. Baccouche, I.; Mlayah, A.; Jemmali, S.; Manai, B.; Essoukri Ben Amara, N. Implementation of a Coulomb counting algorithm for SOC estimation of Li-Ion battery for multimedia applications. In Proceedings of the 2015 IEEE 12th International Multi-Conference on Systems, Signals Devices (SSD15), Sakiet Ezzit Sfax, Tunisia, 16–19 March 2015; pp. 1–6.
6. Xing, Y.J.; He, W.; Pecht, M.; Tsui, K.L. State of charge estimation of lithium-ion batteries using the open-circuit voltage at various ambient temperatures. *Appl. Energy* **2014**, *113*, 106–115. [CrossRef]
7. Feng, F.; Lu, R.G.; Wei, G.; Zhu, C.B. Online estimation of model parameters and state of charge of LiFePO4 batteries using a novel open-circuit voltage at various ambient temperatures. *Energies* **2015**, *8*, 2950–2976. [CrossRef]
8. Waag, W.; Fleischer, C.; Sauer, D.U. Critical review of the methods for monitoring of lithium-ion batteries in electric and hybrid vehicles. *J. Power Sources* **2014**, *258*, 321–339. [CrossRef]
9. Moura, S.J.; Krstic, M.; Chaturvedi, N.A. Adaptive PDE observer for battery SOC/SOH estimation. In Proceedings of the ASME 2012 5th Annual Dynamic Systems and Control Conference joint with the JSME 2012 11th Motion and Vibration Conference, Fort Lauderdale, FL, USA, 17–19 October 2012; pp. 101–110.
10. Tian, Y.; Li, D.; Tian, J.; Xia, B. A comparative study of state-of-charge estimation algorithms for lithium-ion batteries in wireless charging electric vehicles. In Proceedings of the 2016 IEEE PELS Workshop on Emerging Technologies: Wireless Power Transfer (WoW), Knoxville, TN, USA, 4–6 October 2016; pp. 186–190.
11. He, H.; Xiong, R.; Zhang, X.; Sun, F.; Fan, J. State-of-Charge Estimation of the Lithium-Ion Battery Using an Adaptive Extended Kalman Filter Based on an Improved Thevenin Model. *IEEE Trans. Veh. Technol.* **2011**, *60*, 1461–1469.
12. Zhang, C.; Jiang, J.; Zhang, L.; Liu, S.; Wang, L.; Loh, P.C. A Generalized SOC-OCV Model for Lithium-Ion Batteries and the SOC Estimation for LNMCO Battery. *Energies* **2016**, *9*, 900. [CrossRef]
13. Plett, G.L. Extended Kalman filtering for battery management systems of LiPB-based HEV battery packs: Part 1. Background. *J. Power Sources* **2004**, *134*, 252–261. [CrossRef]
14. Plett, G.L. Extended Kalman filtering for battery management systems of LiPB-based HEV battery packs—Part 2. Modeling and identification. *J. Power Sources* **2004**, *134*, 262–276. [CrossRef]
15. Plett, G.L. Extended Kalman filtering for battery management systems of LiPB-based HEV battery packs—Part 3. State and parameter estimation. *J. Power Sources* **2004**, *134*, 277–292. [CrossRef]
16. Verbrugge, M.; Tate, E. Adaptive state of charge algorithm for nickel metal hydride batteries including hysteresis phenomena. *J. Power Sources* **2004**, *126*, 236–249. [CrossRef]
17. Xiong, R.; He, H.W.; Sun, F.C.; Zhao, K. Evaluation on state of charge estimation of batteries with adaptive extended Kalman filter by experiment approach. *IEEE Trans. Veh. Technol.* **2013**, *62*, 108–117. [CrossRef]
18. Chiang, Y.H.; Sean, W.Y.; Ke, J.C. Online estimation of internal resistance and open-circuit voltage of lithium-ion batteries in electric vehicles. *J. Power Sources* **2011**, *196*, 3921–3932. [CrossRef]
19. He, H.W.; Zhang, X.W.; Xiong, R.; Xu, Y.L.; Guo, H.Q. Online model-based estimation of state-of-charge and open-circuit voltage of lithium-ion batteries in electric vehicles. *Energy* **2012**, *39*, 310–318. [CrossRef]

20. Han, J.; Kim, D.; Sunwoo, M. State-of-charge estimation of lead-acid batteries using an adaptive extended Kalman filter. *J. Power Sources* **2009**, *188*, 606–612. [CrossRef]
21. Wang, J.P.; Guo, J.G.; Ding, L. An adaptive Kalman filtering based State of Charge combined estimator for electric vehicle battery pack. *Energy Convers. Manag.* **2009**, *50*, 3182–3186.
22. Charkhgard, M.; Farrokhi, M. State-of-charge estimation for lithium-ion batteries using neural networks and EKF. *IEEE Trans. Ind. Electron.* **2010**, *57*, 4178–4187. [CrossRef]
23. Xiong, R.; Sun, F.C.; Gong, X.Z.; Gao, C.C. A data-driven based adaptive state of charge estimator of lithium-ion polymer battery used in electric vehicles. *Appl. Energy* **2014**, *113*, 1421–1433. [CrossRef]
24. Xiong, R.; Sun, F.C.; Chen, Z.; He, H.W. A data-driven multi-scale extended Kalman filtering based parameter and state estimation approach of lithium-ion polymer battery in electric vehicles. *Appl. Energy* **2014**, *113*, 463–476. [CrossRef]
25. Xia, B.Z.; Wang, H.Q.; Wang, M.W.; Sun, W.; Xu, Z.H.; Lai, Y.Z. A new method for state of charge estimation of lithium-ion battery based on strong tracking cubature Kalman Filter. *Energies* **2015**, *8*, 13458–13472. [CrossRef]
26. Xia, B.Z.; Wang, H.Q.; Tian, Y.; Wang, M.W.; Sun, W.; Xu, Z.H. State of charge estimation of lithium-ion batteries using an adaptive cubature Kalman Filter. *Energies* **2015**, *8*, 5916–5936. [CrossRef]
27. Hu, X.S.; Li, S.B.; Peng, H.E. A comparative study of equivalent circuit models for Li-ion batteries. *J. Power Sources* **2012**, *198*, 359–367. [CrossRef]
28. Xiong, R.; Gong, X.Z.; Mi, C.C.; Sun, F.C. A robust state-of-charge estimator for multiple types of lithium-ion batteries using adaptive extended Kalman filter. *J. Power Sources* **2013**, *243*, 805–816. [CrossRef]
29. Liu, Z.T.; He, H.W. Model-based sensor fault diagnosis of a lithium-ion battery in electric vehicles. *Energies* **2015**, *8*, 6509–6527. [CrossRef]
30. Ioannou, P.A.; Sun, J. *Robust Adaptive Control*; Dover Publications: Mineola, NY, USA, 1996.
31. Ye, G.L.; Smith, P.P.; Noble, J.A. Model-based ultrasound temperature visualization during and following hifu exposure. *Ultrasound Med. Biol.* **2010**, *36*, 234–249. [CrossRef] [PubMed]
32. Taborelli, C.; Onori, S. State of charge estimation using extended Kalman filters for battery management system. In Proceedings of the IEEE International Electric Vehicle Conference (IEVC), Florence, Italy, 17–19 December 2014; pp. 1–8.
33. Yang, S.C.; Deng, C.; Zhang, Y.L.; He, Y.L. State of charge estimation for lithium-ion battery with a temperature-compensated model. *Energies* **2017**, *10*, 1560. [CrossRef]
34. Baccouche, I.; Jemmali, S.; Manai, B.; Omar, N.; Amara, N.E.B. Improved OCV model of a li-ion NMC battery for online SOC estimation using the extended Kalman Filter. *Energies* **2017**, *10*, 764. [CrossRef]